Journal of Power Sources 195 (2010) 5794–5800

Contents lists available at ScienceDirect

Journal of Power Sources

journal homepage: www.elsevier.com/locate/jpowsour

Size effect investigation on battery performance: Comparison between micro- and nano-particles of β-Ni(OH)$_2$ as nickel battery cathode material

M.A. Kiani, M.F. Mousavi *, S. Ghasemi

Department of Chemistry, Tarbiat Modares University, P.O. Box 14115-175, Tehran, Iran

ARTICLE INFO

Article history:
Received 13 October 2009
Received in revised form 22 March 2010
Accepted 26 March 2010
Available online 2 April 2010

Keywords:
Nickel batteries
Sonication process
Surfactant
Nano-particles

ABSTRACT

In this work we report on the comparison between nano- and micro-particles of β-Ni(OH)$_2$ as cathode material of Ni battery. The synthesis of nano- and micro-particles of nickel hydroxide is done by two different procedures: sonication process and stirrer. Nano-particles of β-Ni(OH)$_2$ are synthesized by chemical precipitation from a solution containing $NiCl_2 \cdot 6H_2O$ and surfactant under ultrasonic irradiation. Micro-particles of β-Ni(OH)$_2$ are synthesized by a similar procedure while applying magnetic stirring instead of ultrasonic. The products are characterized by scanning electron microscopy and X-ray powder diffraction. Under the optimized conditions nickel hydroxide nano-particles, with an average particle size of 18 nm, are obtained. Cyclic voltammetric (CV) studies show a pair of well-defined peaks for Ni(OH)$_2$/NiOOH redox reaction, along with faster proton diffusion coefficient and higher oxygen evolution potential for nano-particles of nickel hydroxide compared to that of micro-particles. Electrochemical impedance spectroscopy (EIS) studies of Ni(OH)$_2$ electrodes show that the reaction occurring at the nickel hydroxide is controlled by charge transfer and Warburg diffusion. The β-Ni(OH)$_2$ nano-particles are found to exhibit a superior cycling reversibility and improved capacity when they are used as positive electrode materials of alkaline rechargeable batteries.

1. Introduction

Nickel hydroxide is widely used as the active material for positive electrodes in Ni-based alkaline rechargeable batteries including nickel/cadmium (Ni/Cd), nickel/iron (Ni/Fe), nickel/metal hydride (Ni/MH), and nickel/zinc (Ni/Zn). The high power density, good cycling ability, and relatively low cost of nickel electrodes have made these batteries very competitive for an extended range of applications. There exist two nickel hydroxide polymorphs: α-phase Ni(OH)$_2$ and β-phase Ni(OH)$_2$, which transform into γ-phase NiOOH and β-phase NiOOH, respectively, after full charging. Although α-Ni(OH)$_2$ has higher theoretical electrochemical capacity (433 mAh g^{-1} with an average oxidation state of 3.5 or higher for nickel in the γ-phase) it is very unstable in a strong alkaline medium and easily transforms to the β-phase after a few cycles. β-Phase spherical nickel hydroxide powders are usually used as active materials since the β-phase has a high tap density (2.1–2.2 g cm^{-3}) and good stability in an alkaline electrolyte. However, the β-phase nickel hydroxide has its theoretical capacity limit at 289 m Ahg^{-1}.

Effective charging of the Ni(OH)$_2$ electrode to obtain the maximum capacity depends on particle size, morphology, additives and electrode preparation. Improvement of the nickel hydroxide powder in positive electrodes has the highest priority for increasing the performance of rechargeable alkaline batteries. Many studies have been carried out to improve the performance of the positive electrodes, including: enhancing the stability of the α-phase [1], additives [2], surface modification [3] and nano-sized materials [4,5]. Kohler et al. [6] stated that the intercalation and release of protons into and from the nickel hydroxide host lattice was enhanced by crystal imperfection.

Some of the advantages of the preparation of nanocrystalline material by the ultrasonication method are: more uniform distribution/dispersion of the nano-particles, a marginally higher surface area and better thermal stability and phase purity. In recent years, the fabrication of nano-particles by the general method of sonochemistry has been reported in many published papers and review articles [7–9]. A number of theories have been developed in order to explain how ultrasonic waves cause the formation of materials in nanodimensions. One famous theory regarding the liquid phase refers to the creation, growth and collapse of a bubble that is formed in liquid. This theory claims that very high temperatures (5000–25,000 K) [10] are obtained upon the collapse of the bubble. Since this collapse occurs in less than a nanosecond [11,12], very high cooling rates, in excess of 10^{11} K s^{-1}, are also obtained.

* Corresponding author. Tel.: +98 21 82883474/82883479; fax: +98 21 82883455.
E-mail addresses: mfmousavi@yahoo.com, mousavim@modares.ac.ir (M.F. Mousavi).

0378-7753/$ – see front matter © 2010 Elsevier B.V. All rights reserved.
doi:10.1016/j.jpowsour.2010.03.080

Such high cooling rates hinder the organization and crystallization of the products. More details about the growth of the nuclei and the kinetics have also been reported in related papers [7,13].

One of the preparation methods for nanostructure materials is template method. The most widely used methods for the fabrication of nano-materials are physical or chemical techniques guided by appropriate porous 'hard' templates and versatile 'soft' templates, like surfactants [14]. The hard template approach is effective, but some templates are not easily fabricated and removed. However, surfactant assembly as a soft template shows more versatility, suitable reaction environment and potentials for being applied in molecular engineering [15]. The application of electrostatic interactions between surfactant molecules and charged or polarized metal-oxyprecursors, as the inorganic component, has opened a new way to create metastable modifications of metal oxides [16]. Cetyltrimethylammonium bromide (CTAB) is a cationic surfactant that can form CH_3–CH_3–CH_3–N structure and induce the sphere–rod transition of micelles in aqueous solution when some salts, such as NaCl and Na_2SO_4, are added [17]. Therefore, CTAB can be employed to synthesize materials with special morphologies. Ag nanorods [18], Au nanorods [19], lamellar tin(IV) sulfide [20], SnS nano-wires [21], hydroxyapatite nanostructures [22], PbO_2 and Pb_3O_4 single-crystalline nanorods [23], ZnO nanorods [24], Cu_2O nano-whiskers [25] and γ-Fe_2O_3 nanoparticles [26] have been prepared with CTAB as a 'soft' template.

Following our previous work on electrochemical energy storage systems, such as polyaniline battery [27–34], lead-acid battery [35,36], supercapacitor [37] and sonochemical-assisted synthesis of PbO_2 [9], here we report the synthesis of nickel hydroxide micro- and nano-particles, their characterization, electrochemical studies and application as a cathode material of nickel batteries.

2. Experimental

2.1. Apparatus

A multiwave ultrasonic generator (Sonicator® 3000; Misonix, Inc., Farmingdale, NY, USA), equipped with a converter/transducer and titanium oscillator (horn), 12.5 mm in diameter, operating at 20 kHz with a maximum power output of 600 W, was used for the ultrasonic irradiation. The ultrasonic generator automatically adjusted the power level. The wave amplitude in each experiment was adjusted as needed. A cylindrical two-walled glass cell with an interior volume of 300 mL was used for the sonication of the reaction solution. The solution temperature was kept constant by circulating water from a water bath (Optima, Tokyo, Japan). A home-made centrifuge, with a maximum speed of 8000 rpm, was used for the deposition of dispersed nickel hydroxide. Morphological studies of prepared samples were performed by SEM (Philips XL 30). XRD (Philips X'pert diffractometer) and Cu K_α radiation (λ = 0.15418 nm) were used to study the phase composition of the prepared samples. The CV and EIS measurements were carried out using Galvanostat/Potentiostat Autolab (PGSTAT30) connected to a PC. Electrochemical charge/discharge was measured with a Solartron SI 1470.

2.2. Synthesis of nano- and micro-$Ni(OH)_2$ particles

$NiCl_2{\cdot}6H_2O$ and NaOH were supplied from Scharlau (Spain) and used without any purification. Cationic CTAB surfactant (from Fluka) was used in the synthesis. Doubly distilled water was used throughout. A typical procedure for the formation of nanostructured $Ni(OH)_2$ was as below: 100 mL of 0.1 M $NiCl_2{\cdot}6H_2O$ and 0.8 mM CTAB (approximate critical micelle concentration CMC) were prepared and sonicated for 5 min in a sonication flask. Then, 100 mL of 0.2 M NaOH was added dropwise into the sonication flask over 45 min. Sonication process was carried out at constant wave amplitude and continued up to 1 h. The temperature of the sonication flask was adjusted (at 30 °C) by a water circulator. The precipitate was allowed to settle for 2 h and the colloidal suspensions were centrifuged for 10 min at 7000 rpm and washed with distilled water several times. The centrifugation and washing were performed at the same conditions for products prepared in the absence of surfactant to keep the procedures comparable. The precipitate was dried to constant weight (24 h) in an oven at 70 °C and characterized as $Ni(OH)_2$. Sonication process was performed under constant amplitude (84 μm) and frequency in each experiment. During the experiment, the power of the sonicator was changed depending on the viscosity of the solution and the applied amplitude.

In order to synthesis the micro-$Ni(OH)_2$ particles, the experiment was also performed using magnetic stirring (500 rpm) instead of the sonicator.

2.3. Characterization

XRD was used to study the phase composition of the prepared samples. The sample was scanned from 10° to 80° (2θ) in steps of 0.02°. The average crystallite size was calculated using the Debye–Scherrer formula. All samples were characterized in terms of morphology and particle size by SEM. The average size of particles was obtained using Microstructure Measurement software.

2.4. Electrochemical investigation

The electrochemical properties of the nickel hydroxide electrodes were performed in a three electrode conventional cell. The working electrode for electrochemical tests (CV and EIS) was prepared by incorporating active material paste (90% nickel hydroxide + 10% active carbon pasted by water) into the cavity of Pt electrode (d = 2 mm). The weight of active materials for fabricating electrode in each experiment was exactly equal. A nickel plate and Hg/HgO (1 M KOH) electrode was used as a counter and reference electrode, respectively. The electrolyte used in all electrochemical tests was 6 M KOH solution. The CVs were carried out between 0–0.6 V and 0–0.7 vs. Hg/HgO for micro- and nano-$Ni(OH)_2$, respectively. The EIS experiments were performed at E_{ocp} (a steady state value within 30 min of immersion) over a frequency range of 100 kHz to 10 mHz with a perturbation amplitude of 5 mV, using an ac signal, with at least 7 points per decade which were logarithmically spaced. Data analysis was done based on CNLS method of Boukamp using Zview2 software (Scribner Associates), using an appropriate equivalent circuit described in the text. It should be noted that in all cases, the uncertainty in data fitting was approximately less than 10%. All electrochemical experiments were carried out at room temperature.

The electrodes for charge and discharge studies were prepared as follows: the nickel hydroxides, ultra pure graphite powder (from Merck) and polytetrafluoroethylene (PTFE) (60% water based solution from SUTECH, Iran) were mixed in a weight ratio of 85:10:5 to obtain a paste. The obtained paste was incorporated into nickel network (2.0 cm × 1.0 cm). The obtained nickel electrodes were dried at 70 °C and then pressed under a pressure of 100 kg cm^{-2}. The electrodes were subsequently soaked in 6 M KOH for 24 h. Next, a resulting electrode was coupled with two cadmium electrodes with a capacity in excess of the nickel hydroxide electrodes. Charge and discharge test was carried out under constant current between 0.8 and 1.6 V.

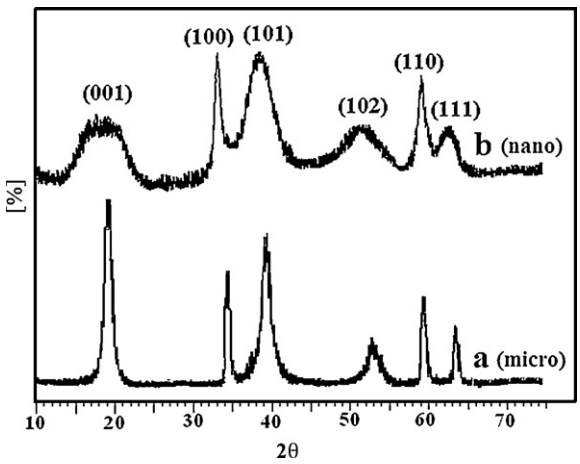

Fig. 1. X-ray diffraction pattern of (a) micro-particles (synthesized by using magnetic stirring) and (b) nano-particles of β-$Ni(OH)_2$ (synthesized by using sonication process).

3. Results and discussion

3.1. XRD studies

XRD was used to study the phase purity of the obtained nickel hydroxide samples. Fig. 1a and b displays the XRD pattern of the nickel(II) hydroxide samples synthesized using magnetic stirring (micro-particles) and sonication process (nano-particles) in the presence of CTAB, respectively. The XRD patterns of the two prepared samples indicate the presence of particles in the form of β-$Ni(OH)_2$, when compared with that of the standard (JCPDS card No. 14-0117), but the width of the peaks is different. No characteristic peaks corresponding to other phases are observed. Fig. 1a has clear and sharp peaks which indicates that β-$Ni(OH)_2$ has big crystallite size. However, as it can be seen in Fig. 1b, peaks (0 0 1), (1 0 1) and (1 0 2) have anomalous broad shapes. The peak positions observed are consistent with those reported previously [5,38]. Comparing the XRD patterns of nano-sized β-$Ni(OH)_2$ with those of spherical β-$Ni(OH)_2$, Huanbo and Zhento reported that nano-sized particles have broader peaks. Peak broadening in β-$Ni(OH)_2$ XRD patterns has often been correlated with the electrochemical activity of the compound. Previous reports have indicated that peaks (0 0 1) and (1 0 l) were especially broad when the nickel hydroxide was more active [39–41]. Delmas and Tessier also considered a correlation between the electrochemical activity and the XRD pattern of nickel hydroxide [39]. Palacine et al. published a useful paper about the structural characterization of nickel hydroxide and its correlation with electrochemical properties [42]. Also, another work from Delmas and coworkers determined this type of pattern to be associated with very poorly crystallized nickel hydroxide, denoted as β_{bc} (bc: badly crystallized) [43]. This material, obtained by the ageing of α-nickel hydroxide, has very broad (0 0 1) and (1 0 1) lines in its XRD pattern, with narrow ($h\,k$ 0) lines. Other phases for nickel hydroxide with a middle structure between α- and β-nickel hydroxide have also been reported [44,45]. However, as can be seen from Fig. 1b, the XRD pattern of this sample is very similar to the β_{bc}-nickel hydroxide reported pattern by Delmas. A broadening of the (1 0 1) line for nanoscale $Ni(OH)_2$ can be seen, which is ascribed to the disordered structure of the material. Thus, the broadening of the (0 0 1) reflection is caused by the smaller crystalline size, as previously reported [6]. The size of the β-$Ni(OH)_2$ nano-particles estimated from the Debye–Scherrer formula is approximately 18 nm.

3.2. SEM studies

Fig. 2 shows the SEM image of the as-prepared $Ni(OH)_2$ by magnetic stirrer. Precipitations were carried out in the absence (Fig. 2a) and presence (Fig. 2b) of CTAB. The morphology of this sample can be seen in the micrograph with the magnification of 2000× (Fig. 2a),

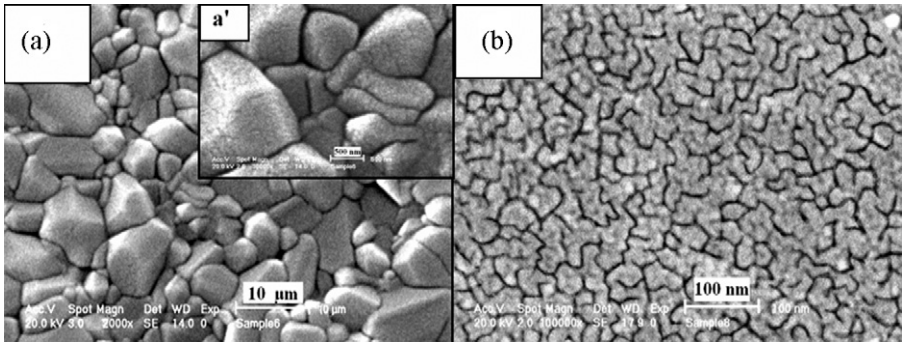

Fig. 2. SEM micrographs of β-$Ni(OH)_2$ micro-particles, synthesized at 30 °C in the absence (a) and (b) presence of 0.8 mM CTAB. Inset (a′) is 10-fold magnification of (a).

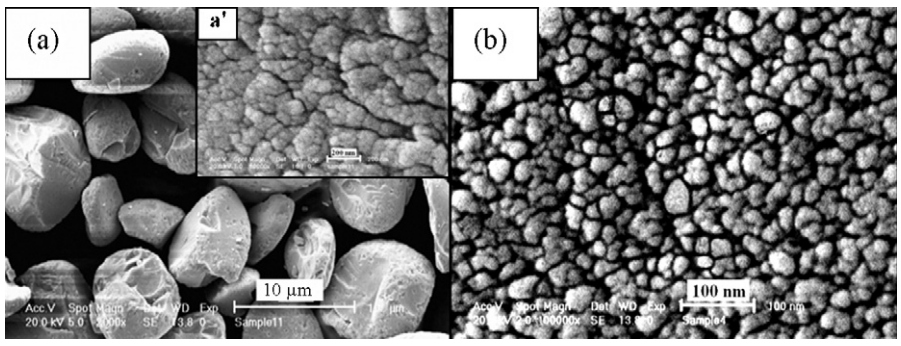

Fig. 3. SEM micrographs of β-$Ni(OH)_2$ nano-particles, synthesized at 30 °C and a wave amplitude of 84 μm, in the (a) absence and (b) presence of 0.8 mM CTAB. Inset (a′) is 5-fold magnification of (a).

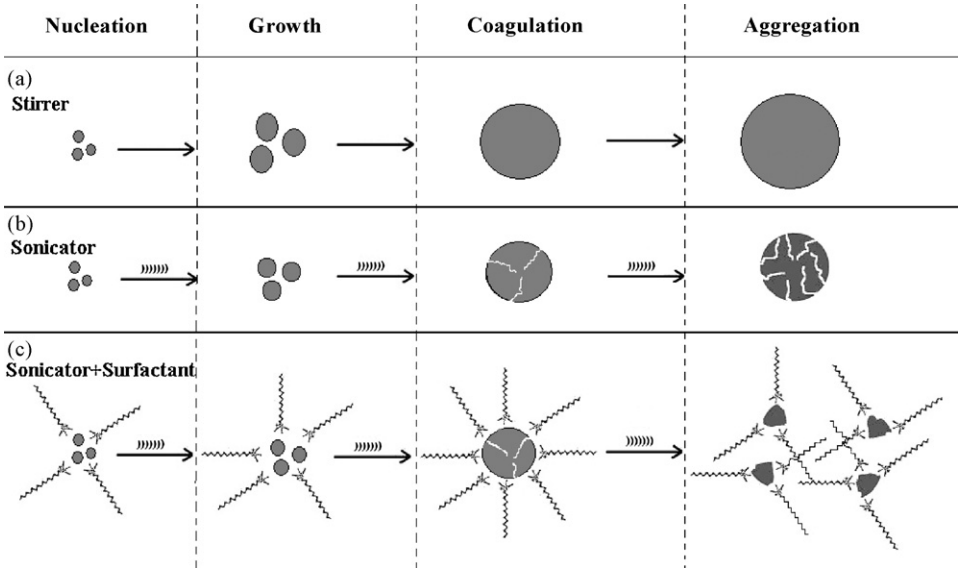

Fig. 4. Schematic illustration of the synthesis process: (a) by magnetic stirring, (b) by sonicator and (c) by sonicator in the presence of CTAB at near CMC.

in which precipitation was carried out without any surfactant, consisting of large sticky particles. Note that this morphology is more like a pavement surface with no space between the grains. The higher magnification (30,000×) presented in Fig. 2a′, shows the lack of separation between the grains, in more detail. In the next step, synthesis was done in the presence of cationic surfactant. Fig. 2b shows the effect of CTAB (0.8 mM) on the nickel hydroxide morphology when prepared using a magnetic stirrer. As can be seen in this figure, CTAB as capping agent inhibits more particle growth therefore a partial separation of the grains is observed.

As it can be seen in Fig. 3a the use of sonication during synthesis results in the formation of smaller particles which is due to induction of more powerful dispersion, consequently, well separated particles are obtained. Higher magnification reveals that each particle is composed of smaller ones (Fig. 3a′). It may be concluded that the ultrasonic waves are useful for separating the particles, but in the absence of capping agents the effect of ultrasonic wave is not efficient for maintaining the smaller particles.

Fig. 3b shows the nanostructured $Ni(OH)_2$ prepared using the sonochemical process assisted by CTAB (0.8 mM). This figure shows that in the presence of CTAB, nickel hydroxide nano-particles are well separated and their size ranges from 5 to 50 nm, with an average of 18 nm (averaged from 70 particles). However, the bigger particles are made of aggregated smaller particles.

CTAB not only provides favorable sites for particulate growth, but also influences the formation process, including nucleation, growth, coagulation and aggregation. Furthermore, the addition of CTAB can affect the nucleation before and during the precipitation process. A schematic depiction of the role of CTAB is proposed in Fig. 4. Particles aggregate in the absence of ultrasonic irradiation, as is shown in Fig. 4a. Employing ultrasonic waves prevents particles from aggregation as appeared some cracks on the surface of particles (Fig. 4b). It seems that particle aggregation is not prohibited by sonication alone. In the presence of CTAB and ultrasonic irradiation (Fig. 4c), a layer of CTAB surrounds the $Ni(OH)_2$ with

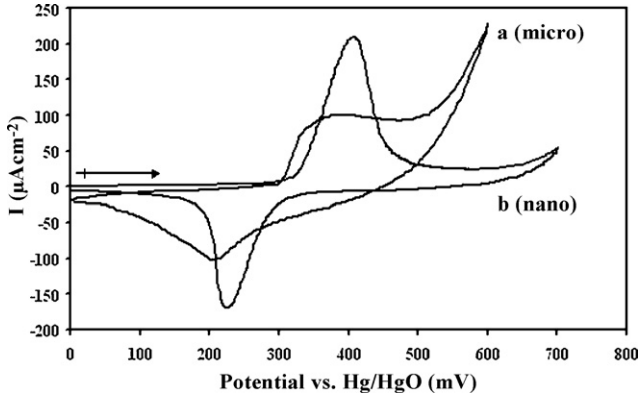

Fig. 5. Cyclic voltammograms of the β-$Ni(OH)_2$: (a) micro-particles and (b) nano-particles of the β-$Ni(OH)_2$ electrode at scan rate of 25 mV s^{-1}.

electrostatic interactions. After nucleation, the surfactant can influence particle growth, coagulation and aggregation. Therefore, CTAB plays an important role in the preparation of these metal hydroxide nano-particles.

3.3. The electrochemical investigation of β-$Ni(OH)_2$

3.3.1. Cyclic voltammetry studies

Fig. 5 shows CVs of micro-particles (Fig. 5a) and nano-particles (Fig. 5b) in 6 M KOH. Both voltammograms show only one anodic peak prior to oxygen evolution and one cathodic peak on the reverse sweep due to the following reaction:

$$\beta\text{-}Ni(OH)_2 \Leftrightarrow \beta\text{-}NiOOH + e^- + H^+ \quad (1)$$

Comparison between CVs of micro-particles (Fig. 5a) and nano-particles (Fig. 5b) shows a pair of well-defined peaks, with higher peak current and wider potential window (116 mV) in oxidation

Table 1
Experimental data from CVs and EIS parameters measurements for micro- and nano-particles of $Ni(OH)_2$ paste electrode.

Particles	E_a (mV)	E_c (mV)	$\Delta E_{a,c}$ (mV)	E_{OER} (mV)	R_c (Ω cm^2)	W (Ω cm^2)	CPE (F cm^{-2})
Micro-particles	390	200	190	450	10.81	11.62	0.02
Nano-particles	408	222	186	566	3.45	4.21	0.07

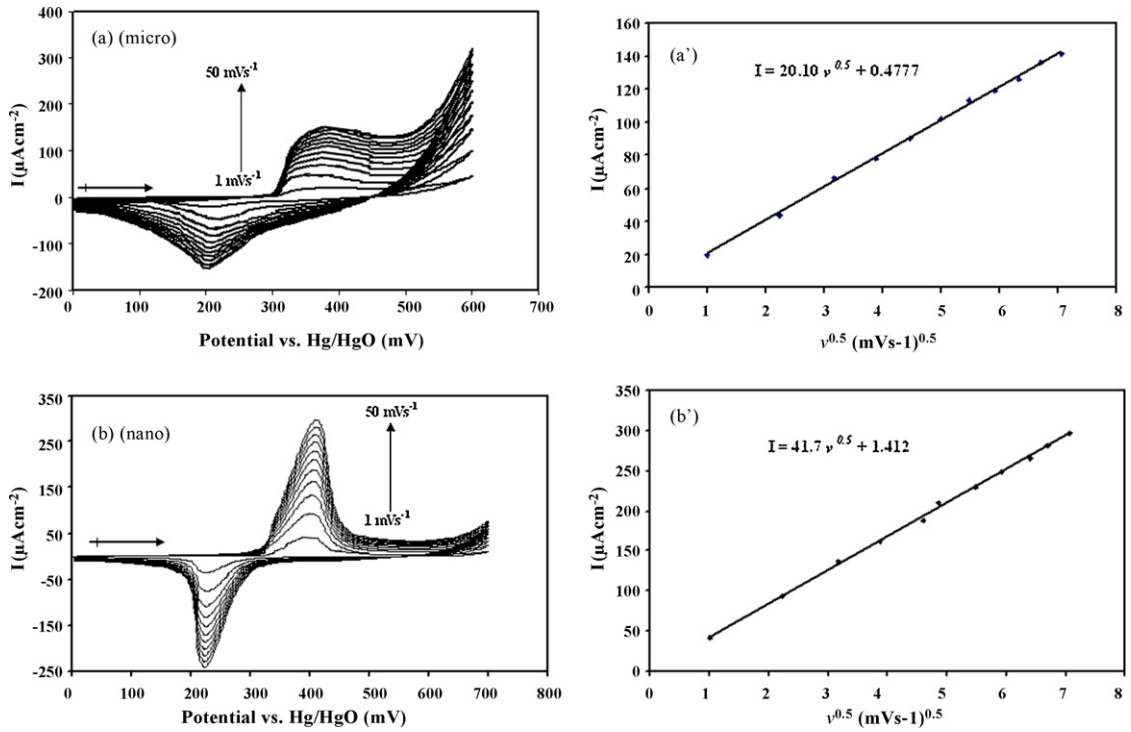

Fig. 6. Cyclic voltammograms of the β-Ni(OH)$_2$: (a) micro-particles and (b) nano-particles at different scan rates (1–50 mV s^{-1}). Linear relationship between anodic peak current and square root of scan rate for the β-Ni(OH)$_2$: (a′) micro-particles and (b′) nano-particles.

direction for nano-particles compared to micro one. So, nano-particles produce more current due to higher surface area and wider potential window which causes the battery performance to improve. In other words, extended positive potential window leads to more charging and therefore produce more capacity. Table 1 summarizes comparison of the electrochemical behavior of micro- and nano-particles of Ni(OH)$_2$ electrode. The charge process of the Ni(OH)$_2$ electrode usually occurs in competition with an oxygen evolution reaction (OER), which limits the electrochemical performance of the nickel hydroxide electrodes. In order to compare the oxygen evolution overpotential for the two types of synthesized Ni(OH)$_2$, the potential at 1 μA on the reverse scan was estimated from the CV at the scan rate of 25 mV s^{-1} (Fig. 5). The oxygen evolution overpotentials were 566 and 450 mV for nano- and micro-particles, respectively.

As is known, the proton diffusion is the rate-determining step in the nickel hydroxide electrode [46] and thereby, the increase in the rate of proton diffusion results in the decrease of electrode polarization. The diffusion coefficient of proton values of the Ni(OH)$_2$ electrode was estimated from the CV tests. Typical CVs for micro- and nano-particles at various scan rates are shown in Fig. 6a and b, respectively. As the scan rate increases, the anodic peak current and the cathodic peak current increase but peaks of potential are almost constant. The characteristic CV parameters obtained from Fig. 6a and b are shown in Fig. 6a′ and b′ as a function of square root of scan rate (ν in mVs^{-1}). In Fig. 6a′ and b′, it can be seen that the anodic peak current vs. $\nu^{0.5}$ plot gives a linear relationship, while anodic peak current vs. ν does not give a linear relationship (not shown here). In semi-infinite diffusion controlled cyclic voltammetry in liquid electrolytes, i vs. $\nu^{0.5}$ gives a linear relationship; for an adsorption process i vs. ν is expected to be linear at different scan rates. The linear relationship between i and $\nu^{0.5}$ suggests that the oxidation of nickel hydroxide is diffusion limited. In the case of semi-infinite diffusion, the peak current i may be expressed by the Sevick equation. According to this equation, it is calculated that the proton diffusion coefficient in micro- and nano-particles are 1.1×10^{-11} and 5.1×10^{-11} cm^2 s^{-1}, respectively, which is in agreement with other reports (1.93×10^{-11} [4] and 1.13×10^{-11} cm^2 s^{-1} [38] for nano-particles). Smaller size, or to say larger real superficial area of nanometer Ni(OH)$_2$ provides more chances for the particles to contact the electrolyte solution; therefore, proton diffusion is enhanced, which in turn will accelerate the electrode reaction.

3.3.2. Electrochemical impedance spectroscopy (EIS)

Electrochemical impedance spectroscopy measurements were carried out for the β-Ni(OH)$_2$ electrodes. The results are shown in Fig. 7 where it can be seen that the Nyquist plots showed a semi-circle in high frequency regions and a linear line in low ones. The characteristics of the electrochemical system can be represented by the electrical equivalent circuit shown as inset of Fig. 7, where R_s is the total resistance of the solution, CPE is the constant phase element, R_c is the charge-transfer resistance of the electrodes, and W is the generalized. The simulated values of the elements for the equivalent circuit are listed in Table 1, where it can be seen that the values of R_c and W of the nano-particles (Fig. 7b) are markedly lower than those of micro-particles (Fig. 7a). Nevertheless, the values of CPE capacitance of nano-particles are higher than micro-particles, which may be due to the fact that nano-sized Ni(OH)$_2$ has a larger efficient active surface area for the electrochemical reactions due to smaller crystals. The results indicate that the nano-particles exhibit a lower resistance to charge-transfer and efficient proton diffusion than that of micro-particles electrode during the electrochemical reactions. This is in agreement with the results of the above CV testing.

3.3.3. Charge/discharge

Fig. 8 shows the discharge curves of β-Ni(OH)$_2$ electrodes at a constant current of 5 mA g^{-1}. As is seen in Fig. 8a, the highest specific discharge capacity of the micro-particles is 241 mAh g^{-1}, while for the nano-particles is 270 mAh g^{-1} (Fig. 8b). This improvement in the specific discharge capacity (12%) can be attributed to the enhancement of surface reactivity as the particle size decreases

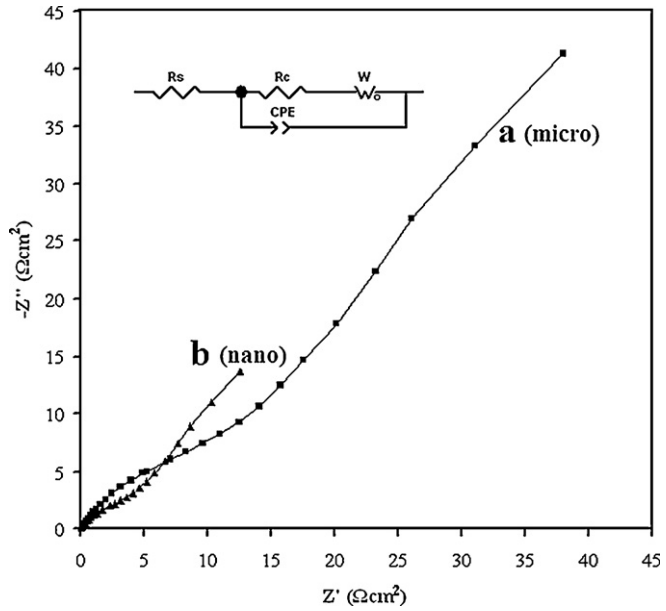

Fig. 7. Nyquist plots of the β-Ni(OH)$_2$: (a) micro-particles and (b) nano-particles in 6 M KOH, OCV, frequency range is between 100 kHz and 10 mHz and corresponding equivalent circuit.

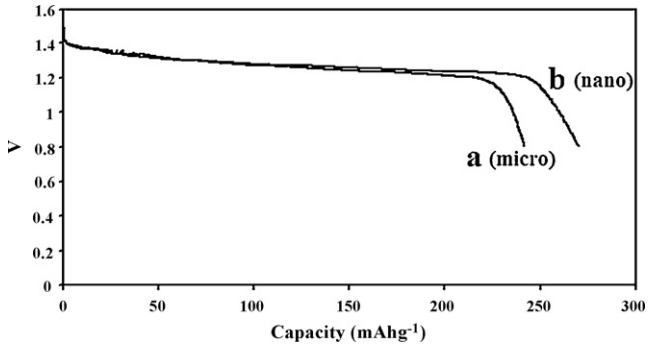

Fig. 8. Discharge curves of the β-Ni(OH)$_2$: (a) micro-particles and (b) nano-particles at 5 mA g^{-1} current.

[47], and lower crystallinity of the nano-particles compared to micro-particles.

The cycle life tests were performed. The results for micro- and nano-particle electrodes are given in Fig. 9a and b, respectively. These two curves have the same trend; showing a significant increase of the capacity which reaches the maximum value after 35 cycles and remains constant up to maximum tested cycles (250 cycles). This capacity increase is due to increasing the number of available active sites in the process. Upon cycling, electrolyte can be more diffused and more active sites become available. However, there is a higher capacity (more than 12%) for nano-particles in all cycles. The specific discharge capacity of the nano-particles that obtained in this work is not higher than the other works [4,5]. At the first look this is a defect, because α-Ni(OH)$_2$ and γ-NiOOH formed do not emerge during cycling. However, the formation of α-Ni(OH)$_2$ and γ-NiOOH is associated with the volume expansion or swelling of the electrode [48], which interferes with effective contact between particles of active material, and this increases the resistance of the electrode reaction and leads to faster capacity decay.

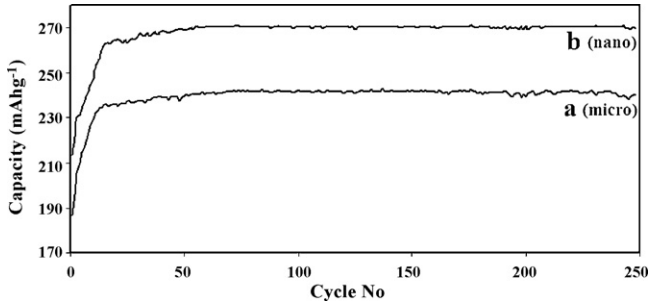

Fig. 9. Cycling performance of the β-Ni(OH)$_2$: (a) micro-particles and (b) nano-particles.

4. Conclusion

This paper described the effect of the size of cathodic materials on Ni battery performance. Synthesis of micro- and nano-particles of nickel hydroxide was done in solution. Surfactant plays an important role in these syntheses by dispersing particles or as-synthesized agglomerated fine particles. Micro- and nano-particles are obtained in the presence of magnetic stirring and ultrasonic wave, respectively. Using ultrasonic waves, dispersed Ni(OH)$_2$ nano-particles were obtained in the presence of CTAB at near CMC. These investigations show that surfactant-mediated method is useful for the preparation of nickel hydroxide nano-particles. Furthermore, this method results in nickel hydroxide nano-particles with a narrow particle distribution and an average particle size of 18 nm.

The nano-sized β-Ni(OH)$_2$ exhibited excellent electrochemical performance, which is markedly superior to micro-sized β-Ni(OH)$_2$, such as allowing the charge process to occur more easily and more reversibly, and oxygen evolution overpotential shifts to a more positive value. The measured value of the diffusion coefficient of proton for the nano-sized β-Ni(OH)$_2$ by cyclic voltammetry testing was 5.1×10^{-11} cm^2 s^{-1}, and the highest discharge capacity measured in the experiments for the nano-sized β-Ni(OH)$_2$ electrode was 270 mAh g^{-1} (12% more than corresponding micro-sized β-Ni(OH)$_2$). Therefore, it can be believed that the nano-sized β-Ni(OH)$_2$ which is synthesized by this method is a promising positive electrode active material for alkaline rechargeable batteries.

Acknowledgements

We gratefully acknowledge the Tarbiat Modares University Research Council and the Iran National Science Foundation (research grant no. 83135) for supporting this work.

References

[1] G. Soler-Illia, M. Jobbágy, A. Regazzoni, M. Blesa, Chem. Mater. 11 (1999) 3140.
[2] L. Jun, L. Rong, W. Jianming, S. Hang, J. Power Sources 79 (1999) 86.
[3] C. Shao-an, W. Leng, Z. Jianqing, C. Chunan, J. Power Sources 101 (2001) 248.
[4] X.J. Han, P. Xu, C.Q. Xu, L. Zhao, Z.B. Mo, T. Liu, Electrochim. Acta 50 (2005) 2763.
[5] H. Zhou, Z. Zhou, Solid State Ionics 176 (2005) 1909.
[6] U. Kohler, C. Antonius, P.B. Uerlein, J. Power Sources 127 (2004) 45.
[7] A. Gedanken, Ultrason. Sonochem. 11 (2004) 47.
[8] D.N. Srivastava, N. Perkas, A. Zaban, A. Gedanken, Pure Appl. Chem. 74 (2002) 1509.
[9] S. Ghasemi, M.F. Mousavi, M. Shamsipur, H. Karami, Ultrason. Sonochem. 15 (2007) 448.
[10] K.S. Suslick, S.B. Choe, A.A. Cichowlas, M.W. Grinstaff, Nature 353 (1991) 414.
[11] R. Hiller, S.J. Putterman, B.P. Barber, Phys. Rev. Lett. 69 (1992) 1182.
[12] B.P. Barber, S.J. Putterman, Nature 352 (1991) 414.
[13] K.S. Suslick, G.J. Price, Annu. Rev. Mater. Sci. 29 (1999) 295.
[14] S. Ghasemi, M.F. Mousavi, M. Shamsipur, Electrochim. Acta 53 (2007) 459–467.
[15] L. Yan, Y. Li, Z.X. Deng, J. Zhuang, X. Sun, Int. J. Inorg. Mater. 3 (2001) 633.
[16] Q. Huo, D.I. Margolese, U. Cielsa, P. Feng, T.E. Gier, P. Sieger, R. Leon, P.M. Petroff, F. Schuth, G.D. Stucky, Nature 368 (1994) 317.
[17] R. Zielinski, S. Ikeda, H. Nomura, S. Kato, J. Colloid Int. Sci. 125 (1988) 497.
[18] N.R. Jana, L. Gearheart, C.J. Murphy, Chem. Commun. (2001) 617.
[19] J. Perez-Juste, L.M. Liz-Marzan, S. Carnie, D.Y.C. Chan, P. Mulvaney, Adv. Funct. Mater. 14 (2004) 571.

[20] J. Li, L. Delmotte, H. Kessler, Chem. Commun. (1996) 1023.
[21] Y. Liu, D. Hou, G. Wang, Chem. Phys. Lett. 379 (2003) 67.
[22] J. Yao, W. Tjandra, Y.Z. Chen, K.C. Tam, J. Ma, B. Soh, J. Mater. Chem. 12 (2003) 3053.
[23] M. Cao, C. Hu, G. Peng, Y. Qi, E. Wang, J. Am. Chem. Soc. 125 (2003) 4982.
[24] X.M. Sun, X. Chen, Z.X. Deng, Y.D. Li, Mater. Chem. Phys. 78 (2002) 99.
[25] Y. Yu, F.P. Du, J.C. Yu, Y.Y. Zhuang, P.K. Wong, J. Solid State Chem. 177 (2004) 4640.
[26] T. Liu, L. Guo, Y. Tao, Y.B. Wang, W.D. Wang, Nanostruct. Mater. 11 (1999) 487.
[27] M.S. Rahmanifar, M.F. Mousavi, M. Shamsipur, J. Power Sources 110 (2002) 229.
[28] H. Karami, M.F. Mousavi, M. Shamsipur, J. Power Sources 117 (2003) 255.
[29] H. Karami, M.F. Mousavi, M. Shamsipur, J. Power Sources 124 (2003) 303.
[30] M.S. Rahmanifar, M.F. Mousavi, M. Shamsipur, M. Ghaemi, J. Power Sources 132 (2004) 296.
[31] M.S. Rahmanifar, M.F. Mousavi, M. Shamsipur, H. Heli, Synth. Met. 155 (2005) 480.
[32] H. Karami, M.F. Mousavi, M. Shamsipur, S. Riahi, J. Power Sources 154 (2006) 298.
[33] Kh. Ghanbari, M.F. Mousavi, M. Shamsipur, Electrochim. Acta 52 (2006) 1514.
[34] Kh. Ghanbari, M.F. Mousavi, M. Shamsipur, H. Karami, J. Power Sources 170 (2007) 513.
[35] S. Ghasemi, M.F. Mousavi, H. Karami, M. Shamsipur, S.H. Kazemi, Electrochim. Acta 52 (2006) 1596.
[36] H. Karami, M. Shamsipur, S. Ghasemi, M.F. Mousavi, J. Power Sources 164 (2007) 896.
[37] H.R. Ghenaatian, M.F. Mousavi, S.H. Kazemi, M. Shamsipur, Synth. Met. 159 (2009) 1717.
[38] H.B. Zhou, Z.T. Zhou, Chin. J. Chem. 24 (2006) 37.
[39] C. Delmas, C. Tessier, J. Mater. Chem. 7 (1997) 1439.
[40] M.C. Bernard, R. Cortes, M. Keddam, H. Takenouti, P. Bernard, S. Senyarich, J. Power Sources 63 (1996) 247.
[41] K. Watanabe, T. Kikuoka, N. Kumagai, J. Appl. Electrochem. 25 (1995) 219.
[42] M.C. Cabanas, J.R. Carvajal, J.C. Vazqueza, M.R. Palacin, J. Mater. Chem. 16 (2006) 2925.
[43] C. Faure, C. Delmas, M. Fouassier, J. Power Sources 35 (1991) 279.
[44] M. Rajamathi, G.N. Subbannab, P.V. Kamatha, J. Mater. Chem. 7 (1997) 2293.
[45] M. Rajamathi, P.V. Kamath, R. Seshadri, J. Mater. Chem. 10 (2000) 503.
[46] S. Motupally, C.C. Streiz, W.J. Weidner, J. Electrochem. Soc. 145 (1998) 29.
[47] P. Poizot, S. Laruelle, S. Grugeon, L. Dupont, J.M. Tarascon, Nature 407 (2000) 496.
[48] W.-K. Hu, D. Noreus, Chem. Mater. 15 (2003) 974.